Mapping the Efficiency for a Hydrostatic Transmission

Noah D. Manring
Rolf Fluid Power Laboratory,
Mechanical and Aerospace
Engineering Department,
University of Missouri,
Columbia, MO 65211
e-mail: ManringN@missouri.edu

Efficiency maps have long been used by engineers to understand the topographical behavior of their machinery. Most commonly, efficiency maps have been generated for internal combustion engines, where the torque–speed curve for the engine shows the wide-open-throttle line with constant efficiency lines drawn beneath this maximum operating limit. From such maps, engineers have been able to determine the most efficiency operating point for the engine, given a desired output power (torque and speed). There currently exists a great interest in using hydrostatic transmissions for improving the operating efficiency of an internal combustion engine. However, efficiency maps for hydrostatic transmissions, similar to efficiency maps for internal combustion engines, do not exist in the literature and therefore it is difficult to assess the overall efficiency gains that are achieved when using a hydrostatic transmission in these applications. This paper proposes a method for generating efficiency maps for hydrostatic transmissions, and presents a typical set of maps that may be used as a first approximation for assessing transmission efficiency. The results of this paper are nondimensional and are generalized for a transmission of any size. As shown in this research, there are regimes of transmission operation in which the efficiency is nearly independent of either the output torque, or the output speed. Furthermore, it is shown that maximum operating efficiencies typically exist at high output speeds, and mid-to-high output torques.
[DOI: 10.1115/1.4032289]

Introduction

Background. A hydrostatic transmission is a continuously variable transmission (CVT) that facilitates power transfer without using a discrete number of gear ratios. These transmissions are frequently used to propel off-highway machinery for the construction and earth moving industry, as well as the lawn and garden industry. CVT technology has also become popular in the on-highway automotive industry as it allows the internal combustion engine of the vehicle to operate at its most efficient operating point for a given power requirement of the vehicle. Some have estimated that a CVT can improve the fuel efficiency of the internal combustion engine by as much as 60% [1]. As a result of this potential fuel savings, hybrid vehicle technology which uses a CVT has emerged in several automotive sectors. For small vehicles electric CVTs have been employed while larger utility vehicles have adopted hydraulic CVTs (also called hydrostatic transmissions). In all of this work, the focus has been on improving the operating efficiency of the engine; however, little attention has been paid to the operating efficiency of the CVT itself. This oversight becomes especially important for CVTs that utilize hydrostatic transmissions as these transmissions do not enjoy a reputation for being extremely efficient themselves. Even so, the hydrostatic transmission exhibits other characteristics that make it an attractive replacement for electric CVTs which are more commonly used in passenger vehicles. For example, hydrostatic components are much less expensive and have better energy-storage options than their electrical counterparts. For example, hydraulic accumulators are better suited for rapid power discharge as compared to electric batteries. In order to increase the penetration of CVTs into the automotive market, the Environmental Protection Agency (EPA) has been sponsoring programs for the development of hydraulic hybrid-vehicles [2]. The EPA deems a hydrostatic CVT as being more cost effective than an electric CVT; however, among other things the efficiency comparison between these two transmissions has not been well established. In order to understand the efficiency characteristics of the hydrostatic transmission, it would be useful to have conventional maps of the overall efficiency characteristics of these machines. These types of efficiency maps are common for internal combustions engines, but they are not common for hydrostatic transmissions. The focus of this paper is to describe a method for generating such efficiency maps for hydrostatic transmissions, and to present a typical set of maps that may be used to give a first approximation for the behavior and efficiency characteristics of these machines.

Literature Review. Examples of electric CVT research include work done by Pfiffner and colleagues [3] in which a numerical method is used to model the transmission and to optimize the engine efficiency. This work does not model the transmission in detail but considers the efficiency characteristics of the engine. Like other research that has been conducted in this area, the efficiency of the transmission is assumed to be 100%. Pfiffner concludes that fuel consumption may be reduced by as much as 5% using the proposed method of control. Mapelli and colleagues [4] have considered a transmission similar to that of Pfiffner; however, they have given greater attention to the losses in the transmission itself. This work does not present a comparison of the CVT design with a more conventional design and so it is difficult to know whether or not any improvements have been made. Kessels et al. [5] provided more details in the description of their electric CVT design which consists of two motor–generators with power electronics being used to regulate battery power input and output. By considering the efficiency of all components, Kessels and colleagues conclude that it may not always be best to operate the engine at its point of maximum efficiency for a given power demand since global optimal vehicle efficiency may not correspond with this operating point. Ehsani and colleagues [6] have provided a more comprehensive textbook for considering the fundamental building block of electric CVTs.

Hydraulic CVTs have been studied by Kumar and Ivantysynova [7] in which a continuously variable pump and motor are used with an accumulator to provide a capacity for storing braking energy as well as optimizing the efficiency of the engine.

Contributed by the Dynamic Systems Division of ASME for publication in the Journal of Dynamic Systems, Measurement, and Control. Manuscript received March 11, 2015; final manuscript received November 30, 2015; published online January 12, 2016. Assoc. Editor: Luis Alvarez.

This work concludes that the hydraulic CVT can reduce the fuel consumption of a comparable electric CVT by over 16%. A fair amount of work has also been done on hydraulic hybrid-technologies at the University of Missouri. Dirck [8] has modeled a simple hydraulic hybrid which utilizes a parallel discrete-transmission to show that the fuel consumption of a typical automobile may be reduced by 37% for city driving and 14% for highway driving. Vermillion [9] has modeled a more complex hydraulic CVT which utilizes a pressure compensated pump, and a variable displacement motor while considering the efficiency characteristics of the hydraulics. In his work, Vermillion has shown that fuel consumption may be reduced by just 1.28% in the city, and by over 22% for highway driving. Al-Ghrairi [10] has shown that the transmission modeled by Vermillion can be designed within a compact space while ensuring that all transmission components, including complex gear arrangements, can satisfy the safety-factor requirements that are typical of modern machine design practice. As it turns out, all of this work has been conducted without generating efficiency maps that may lend insight into the optimal operating conditions of the transmission itself. The work conducted in this present research paper is aimed at addressing this deficiency.

Objectives. Efficiency maps have long been used by engineers to understand the topographical behavior of their machinery. Most commonly, efficiency maps have been generated for internal combustion engines, where the torque–speed curve for the engine shows the wide-open-throttle line with constant efficiency lines drawn beneath this maximum operating limit. From such maps, engineers have been able to determine the most efficiency operating point for the engine, given a desired output power (torque and speed). There currently exists a great interest in using hydrostatic transmissions for improving the operating efficiency of an internal combustion engine. However, efficiency maps for hydrostatic transmissions, similar to efficiency maps for internal combustion engines, do not exist in the literature and therefore it is difficult to assess the overall efficiency gains that are achieved when using a hydrostatic transmission in these applications. This paper proposes a method for generating efficiency maps for hydrostatic transmissions and presents a typical set of maps that may be used as a first approximation for assessing transmission efficiency. The results of this paper are nondimensional and are generalized for a transmission of any size. As shown in this research, there are regimes of transmission operation in which the efficiency is nearly independent of either the output torque, or the output speed. Furthermore, it is shown that maximum operating efficiencies typically exist at high output speeds, and mid-to-high output torques.

Transmission Description

Figure 1 shows a schematic for a hydrostatic transmission. As shown in this figure, the transmission is comprised of two basic components: a pump and a motor. In the application of this transmission, the pump input-shaft is driven by either an electric motor or an internal combustion engine and is used to covert rotational mechanical-power into fluid power. The fluid power is received downstream by the motor which then reconverts the fluid power to rotational mechanical-power at the output shaft of the motor. The amount of fluid power sent to the motor is regulated by the swash-plate angle of the pump. This swash-plate angle is shown in Fig. 1 using the symbol $\hat{\alpha}$. It will be shown later that the discharge volumetric flow rate from the pump Q_p is proportional to the swash-plate angle. Figure 1 also shows that the hydrostatic transmission has a high-pressure side and a low-pressure side. The high-pressure side has fluid pressured to the level noted by the symbol P. All pressures in the circuit are referenced from the low-pressure side which is shown in Fig. 1 with pressure of zero (as a reference). The volumetric flow rate across the hydrostatic motor is shown in Fig. 1 by the symbol Q_m. The maximum volumetric displacement for the pump is shown in Fig. 1 by the symbol V_p and the fixed displacement for the motor is shown by the symbol V_m.

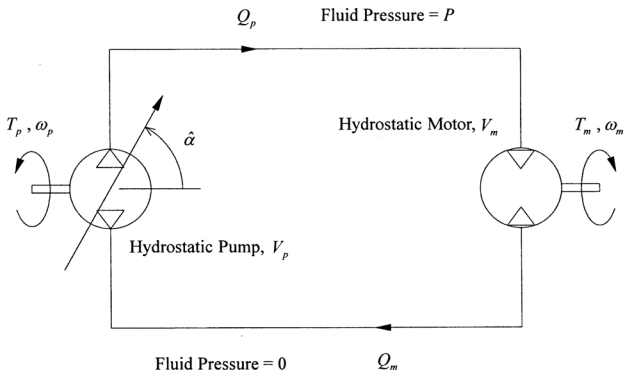

Fig. 1 Schematic of the hydrostatic transmission

Figure 1 is presented in its concept form. The author acknowledges that an actual hydrostatic transmission is more complex than this schematic would suggest, including an auxiliary charge circuit to provide makeup flow to the loop, crossover relief valves for safety, loop flushing valves for cooling, and a reservoir for receiving leakage flow and for supplying makeup flow to the charge circuit. For a more detailed diagram of an actual transmission, the reader is referred to standard texts on this subject [11].

The overall efficiency for the hydrostatic transmission is simply given by the ratio of the power output to the power input as shown in the following equation:

$$\eta = \frac{T_m \omega_m}{T_p \omega_p} \tag{1}$$

where the input torque on the pump shaft is given by T_p and the constant shaft speed for the pump is ω_p. The output torque on the motor shaft is T_m and the varying shaft speed for the motor is given by ω_m. The transmission efficiency shown in Eq. (1) may also be expressed as

$$\eta = \frac{P Q_p}{T_p \omega_p} \times \frac{T_m \omega_m}{P Q_p} = \eta_p \times \eta_m \tag{2}$$

In this expression, P is the pressure in the high-pressure side of the transmission, Q_p is the volumetric flow rate generated by the pump, and η_p and η_m are the efficiencies of the pump and motor, respectively. In other words, the overall efficiency of the hydrostatic transmission is simply given by the product of the efficiencies for both the pump and the motor. These efficiencies will be analyzed and modeled in the "Analysis and Modeling" section of this paper.

Note: A reviewer for this paper has noted that experimental results may be used directly to map the efficiency of a hydrostatic transmission. This reviewer is certainly correct; however, it is difficult to hold the efficiency of the transmission constant, and therefore constant-efficiency lines, which are desired in this research, are not easily produced in the laboratory. Furthermore, an objective of this work is to produce results that can be easily applied to the analysis of the CVT systems. In order to satisfy these needs, the following work will present a hybrid model that depends upon analysis, modeling, and experimental work.

Analysis and Modeling

Pump Analysis. To analyze the efficiency of the hydrostatic transmission, it is useful to begin with a consideration of the pump, which does the job of converting rotational mechanical-power into fluid power. The input power to the pump is given by the input-shaft torque T_p, times the angular velocity of the

shaft ω_p. The output power of the pump is given by the discharge pressure of the pump P, times the discharge volumetric-flow rate Q_p. Using these definitions, the overall efficiency of the pump may be expressed

$$\eta_p = \frac{P\,Q_p}{T_P\,\omega_p} \tag{3}$$

In order to evaluate this expression, quantities for the volumetric-flow rate and the shaft torque must be determined. The following paragraphs will be used to do this.

Figure 2 shows a schematic of the pump, including volumetric-flow rates, mass-flow rates, and the other relevant parameters associated with converting mechanical power into fluid power. From the conservation of mass, it may be shown that

$$\dot{m}_d = \dot{m}_i - \dot{m}_{ld} - \dot{m}_{li} \tag{4}$$

where $\dot{m}_d$ is the mass-flow rate on the discharge side, $\dot{m}_i$ is the mass-flow rate on the inlet side, $\dot{m}_{ld}$ is the mass-flow rate of leakage from the discharge side, and $\dot{m}_{li}$ is the mass-flow rate of leakage from the intake side of the pump. Recognizing that the mass-flow rate is related to the volumetric-flow rate by the expression $\dot{m} = \rho\,Q$, where ρ is the fluid mass–density, Eq. (4) may be written in terms of volumetric-flow rates as

$$Q_p = \frac{\rho_i}{\rho_d}\,(Q_i - Q_{li}) - Q_{ld} \tag{5}$$

where ρ_i is the fluid density on the inlet side of the pump and ρ_d is the fluid density on the discharge side of the pump.

From the definition of the fluid bulk modulus-of-elasticity [11], it may be shown that density of the fluid is given by

$$\rho = \rho_o \mathrm{Exp}\left(\frac{P}{\beta}\right) \tag{6}$$

where ρ_o is the fluid density at zero gauge-pressure, P is the fluid gauge-pressure, and β is the fluid bulk modulus. Using this equation, it may be shown that

$$\frac{\rho_i}{\rho_d} = \mathrm{Exp}\left(-\frac{P}{\beta}\right) \approx 1 - \frac{P}{\beta} \tag{7}$$

where the inlet pressure to the pump P_i has been taken as zero gauge-pressure. Assuming that the pump is completely filled at the inlet, the volumetric flow rate at inlet is given by

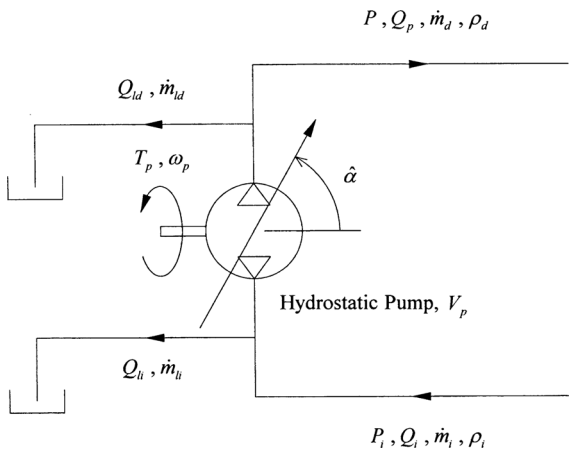

Fig. 2 Schematic of the pump, showing the mass and volumetric flow rates

$$Q_i = V_p\,\omega_p\,\hat{\alpha} + Q_{li} \tag{8}$$

where V_p is the maximum volumetric displacement of the pump, $\hat{\alpha}$ is the normalized swash-plate angle of the pump which ranges from $-1 < \hat{\alpha} < +1$, and Q_{li} is the leakage that occurs on the inlet side of the pump. In order to complete the analysis for the discharge volumetric-flow rate of the pump, a good model for the leakage on the discharge side needs to be established. In most cases, the leakage from the discharge side of the pump occurs through flow that is characterized by a low Reynolds-number. This kind of flow is proportional to the pressure in the discharge line and is inversely proportional to the fluid viscosity. However, it is conceivable that some of this leakage occurs through a flow rate that is characterized by a high Reynolds-number in which case the flow is proportional to the square root of the discharge pressure. Combining both types of flow, a good and reasonable model for the leakage on the discharge side of the pump may be written as

$$Q_{ld} = K_1'\,\frac{1}{\mu}\,P + K_2'\,\sqrt{P} \tag{9}$$

where K_1' and K_2' are coefficients that must be determined from experiments, and μ is the absolute fluid–viscosity which exhibits a strong dependence on the operating temperature of the fluid.

Substituting Eqs. (7)–(9) into Eq. (5) produces the following expression for the discharge volumetric-flow rate of the pump:

$$Q_p = \left(1 - \frac{P}{\beta}\right) V_p\,\omega_p\,\hat{\alpha} - K_1'\,\frac{1}{\mu}\,P - K_2'\,\sqrt{P} \tag{10}$$

This result will be used for modeling the volumetric flow rate of the fluid as it contributes to the pump efficiency shown in Eq. (3).

The torque on the input-shaft of the pump is a combination of a theoretically perfect-torque plus the torque that is required to overcome the internal friction of the pump. In this case, the following model is proposed for the input torque on the shaft of the pump:

$$T_p = V_p\,\hat{\alpha}\,P + V_p\,\hat{\alpha}\,P\,\mu_{sp} + D_p' \tag{11}$$

where $V_p\,\hat{\alpha}\,P$ represents the idealized torque [12,13], D_p' is a fixed starting torque that must be overcome to initially move the pump shaft, and μ_{sp} is an average coefficient-of-friction that exists within the pump.

The coefficient of friction has been modeled using the well-known Stribeck curve [13] shown in Fig. 3. This figure illustrates the changing coefficient of friction as it varies with the absolute fluid–viscosity μ, the linear sliding velocity U, and the normal load per unit width W.

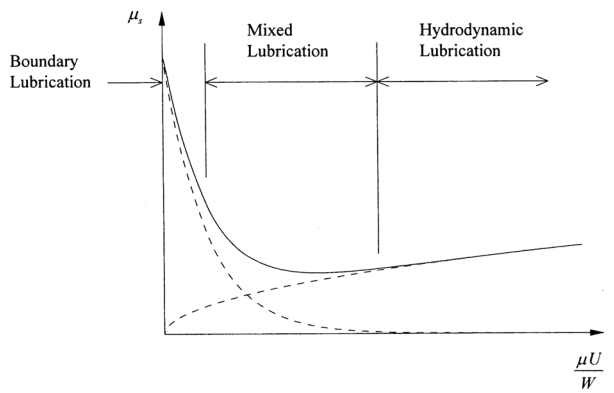

Fig. 3 The Stribeck curve for modeling the coefficient-of-friction

Three types of lubrication are noted in the figure: (1) boundary lubrication in which metal-to-metal contact dominates the friction, (2) mixed lubrication in which a partial fluid-film thickness is separating the contact surfaces, and (3) fully hydrodynamic lubrication in which the contact surfaces are completely separated from each other by a fluid-film thickness. Using textbook lubrication analysis [11–13], it may be shown that fully hydrodynamic lubrication is proportional to the square root of $\mu U/W$. Unfortunately, there are no closed-form expressions available to describe the transition of friction as it move from boundary, to mixed, to fully hydrodynamic lubrication. Previous research by the author [14] has simply modeled this transition using an exponential decay which has correlated well with experiments. Based upon this approach, the coefficient-of-friction as modeled by the Stribeck curve may be represented using the following mathematical expression:

$$\mu_{sp} = A_p \operatorname{Exp}\left(-B'_p \frac{\mu U}{W}\right) + C'_p \sqrt{\frac{\mu U}{W}} \tag{12}$$

In this result, the coefficients A_p, B'_p, and C'_p must be determined from experiments and the two terms on the right-hand side of this equation are schematically shown by the two dashed lines in Fig. 3. The solid line in Fig. 3 represents the left-hand side of this equation. To apply the Stribeck curve to the pump, the linear sliding velocity U will be replaced by the angular shaft velocity ω_p. In addition to this, the load per unit width will be replaced by $\hat{\alpha} P$ which is proportional to the torque on the shaft. In other words, the coefficient-of-friction shown in Eq. (11) is given by

$$\mu_{s_p} = A_p \operatorname{Exp}\left(-B'_p \frac{\mu \omega_p}{\hat{\alpha} P}\right) + C'_p \sqrt{\frac{\mu \omega_p}{\hat{\alpha} P}} \tag{13}$$

Again, the coefficients in this equation are determined from experimental studies.

Substituting Eq. (13) into Eq. (11) produces the following expression for the torque on the input-shaft of the pump:

$$T_p = V_p \hat{\alpha} P + V_p \hat{\alpha} P \left[A_p \operatorname{Exp}\left(-B'_p \frac{\mu \omega_p}{\hat{\alpha} P}\right) + C'_p \sqrt{\frac{\mu \omega_p}{\hat{\alpha} P}}\right] + D'_p \tag{14}$$

This equation is to be used for modeling the shaft torque as it contributes to the overall pump efficiency as shown in Eq. (3).

It will be useful to consider the previous equations in a nondimensional form. In order to create these forms, the following definitions will be used:

$$Q_p = \hat{Q}_p V_p \omega_p, \quad P = \hat{P} P_{\max}, \quad T_p = \hat{T}_p V_p P_{\max} \tag{15}$$

where symbols with carets are nondimensional. Substituting these definitions into Eq. (3) produces the following result for pump efficiency:

$$\eta_p = \frac{\hat{P} \hat{Q}_p}{\hat{T}_P} \tag{16}$$

Similarly, using Eqs. (10) and (15) the nondimensional flow rate may be expressed as

$$\hat{Q}_p = \hat{\alpha} - K_0 \hat{P} \hat{\alpha} - K_1 \hat{P} - K_2 \sqrt{\hat{P}} \tag{17}$$

where

$$K_0 = \frac{P_{\max}}{\beta}, \quad K_1 = \frac{K'_1 P_{\max}}{V_p \omega_p \mu} \quad \text{and} \quad K_2 = \frac{K'_2 \sqrt{P_{\max}}}{V_p \omega_p} \tag{18}$$

Each of these coefficients is nondimensional. Finally, using Eqs. (14) and (15), the nondimensional torque on the input shaft of the pump may be expressed as

$$\hat{T}_p = \hat{\alpha} \hat{P} + A_p \hat{\alpha} \hat{P} \operatorname{Exp}\left(\frac{-B_p}{\hat{\alpha} \hat{P}}\right) + C_p \sqrt{\hat{\alpha} \hat{P}} + D_p \tag{19}$$

where

$$B_p = B'_p \frac{\mu \omega_p}{P_{\max}}, \quad C_p = C'_p \sqrt{\frac{\mu \omega_p}{P_{\max}}}, \quad D_p = \frac{D'_p}{V_p P_{\max}} \tag{20}$$

Each of these coefficients is nondimensional and must be determined from experiments, along with A_p. Once the coefficients have been determined from experiments, an efficiency map for the pump may be drawn by finding a simultaneous solution for Eqs. (16), (17), and (19). This exercise will be carried out in the "Results and Discussion" section of this paper.

Motor Analysis. Similar to analyzing the pump efficiency for the hydrostatic transmission, it is useful to develop an expression for the efficiency of the motor. The motor does the job of converting fluid power into rotational mechanical-power at the output shaft. The input power to the motor is given by the supply pressure, P, times the supply flow from the pump Q_p. The output power of the motor is given by the motor shaft torque, T_m, times the angular velocity of the motor shaft ω_m. Using these definitions, the overall efficiency of the motor may be expressed as

$$\eta_m = \frac{T_m \omega_m}{P Q_p} \tag{21}$$

In order to evaluate this expression, quantities for the shaft torque and the motor shaft speed must be determined. The following paragraphs will be used to do this.

The angular velocity of the motor shaft is determined by the volumetric flow rate that passes through the motor. This relationship is simply given by

$$\omega_m = \frac{Q_m}{V_m} \tag{22}$$

where Q_m is the volumetric flow rate that passes through the motor and V_m is the fixed volumetric displacement of the motor. The volumetric flow rate that passes through the motor is given by

$$Q_m = Q_p - Q_l \tag{23}$$

where Q_p is the volumetric flow rate from the pump given in Eq. (10) and Q_l is the leakage that occurs on the intake side of the motor. Similar to the pump, this leakage may be modeled as a combination of high and low Reynolds-number flow

$$Q_l = K'_3 \frac{1}{\mu} P + K'_4 \sqrt{P} \tag{24}$$

where K'_3 and K'_4 are coefficients that must be determined from experiments. Combining Eqs. (10) and (22)–(24) produces the following expression for the angular velocity of the motor output shaft:

$$\omega_m = \left(1 - \frac{P}{\beta}\right) \frac{V_p}{V_m} \omega_p \hat{\alpha} - \frac{K'_1}{V_m} \frac{1}{\mu} P - \frac{K'_2}{V_m} \sqrt{P} - \frac{K'_3}{V_m} \frac{1}{\mu} P - \frac{K'_4}{V_m} \sqrt{P} \tag{25}$$

This equation will be simplified using nondimensional analysis in a subsequent paragraph.

Similar to the torque on the pump shaft, the torque on the motor shaft may be modeled as a combination of idealized torque minus

torque losses due to friction-type loads. For the motor shaft, the following torque equation will be used for this research:

$$T_m = V_m P - V_m P \mu_{sm} - D'_m - E' \omega_m \tag{26}$$

In this equation, the idealized torque is given by $V_m P$, the torque loss due to the friction between sliding parts is given by $V_m P \mu_{sm}$ where μ_{sm} is a coefficient of friction that depends upon the operating conditions of the motor, D'_m is the required starting torque for the motor, and E' is a coefficient which describes "windage" losses in the motor which are proportional to the angular shaft speed of the machine. Using the general form of the Stibeck curve shown in Fig. 3, the coefficient of friction within the machine may be expressed as

$$\mu_{sm} = A_m \operatorname{Exp}\left(-B'_m \frac{\mu \omega_m}{P}\right) + C'_m \sqrt{\frac{\mu \omega_m}{P}} \tag{27}$$

Substituting this result into Eq. (26) produces the following result for the torque on the motor shaft:

$$T_m = V_m P - V_m P \left[A_m \operatorname{Exp}\left(-B'_m \frac{\mu \omega_m}{P}\right) + C'_m \sqrt{\frac{\mu \omega_m}{P}}\right] - D'_m - E' \omega_m \tag{28}$$

This equation is to be used for modeling the shaft torque as it contributes to the overall motor efficiency as shown in Eq. (21).

In order to nondimensionalize the previous equations, it will be useful to define the following relationships:

$$\omega_m = \hat{\omega}_m \frac{V_p}{V_m} \omega_p, \quad T_m = \hat{T}_m V_m P_{\max}, \quad Q_p = \hat{Q}_p V_p \omega_p, \quad P = \hat{P} P_{\max} \tag{29}$$

where symbols with carets are nondimensional. Substituting these definitions into Eq. (21) produces the following result for the motor efficiency:

$$\eta_m = \frac{\hat{T}_m \hat{\omega}_m}{\hat{P} \hat{Q}_p} \tag{30}$$

Similarly, the nondimensional shaft speed for the motor may be expressed using Eq. (25) and the definitions in Eq. (29). This result is given by

$$\hat{\omega}_m = \hat{\alpha} - K_0 \hat{\alpha} \hat{P} - (K_1 + K_3) \hat{P} - (K_2 + K_4) \sqrt{\hat{P}} \tag{31}$$

where K_0, K_1, and K_2 are presented in Eq. (18) and the two new coefficients in Eq. (31) are given by

$$K_3 = \frac{K'_3 P_{\max}}{V_p \omega_p \mu} \quad \text{and} \quad K_4 = \frac{K'_4 \sqrt{P_{\max}}}{V_p \omega_p} \tag{32}$$

Again, each of these coefficients is nondimensional and must be determined from experiments. Continuing this analysis, it may be observed from Eqs. (28) and (29) that the nondimensional form for the motor shaft torque is given by

$$\hat{T}_m = \hat{P} - A_m \hat{P} \operatorname{Exp}\left(-B_m \frac{\hat{\omega}_m}{\hat{P}}\right) - C_m \sqrt{\hat{\omega}_m \hat{P}} - D_m - E \hat{\omega}_m \tag{33}$$

where

$$B_m = B'_m \frac{\mu \omega_p}{P_{\max}} \frac{V_p}{V_m}, \quad C_m = C'_m \sqrt{\frac{\mu \omega_p}{P_{\max}} \frac{V_p}{V_m}}, \quad D_m = \frac{D'_m}{V_m P_{\max}}, \quad E = E' \frac{\omega_p}{P_{\max}} \frac{V_p}{V_m^2} \tag{34}$$

These coefficients are also nondimensional and must be determined from experiments along with the coefficient A_m. Once the coefficients have been determined, an efficiency map for the motor may be drawn by finding a simultaneous solution for Eqs. (30), (31), and (33). This exercise will be carried out in the "Results and Discussion" section of this paper.

Transmission Analysis. The overall efficiency of the hydrostatic transmission has been presented in Eq. (1) of this paper. Using this equation with the nondimensional definitions presented in Eqs. (15) and (29), the overall efficiency of the transmission may be written as

$$\eta = \frac{\hat{T}_m \hat{\omega}_m}{\hat{T}_p} \tag{35}$$

where the nondimensional input torque on the pump is given in Eq. (19), the nondimensional shaft speed of the motor is presented in Eq. (31), and the nondimensional torque on the motor shaft is given in Eq. (33). These three equations, with Eq. (35), create four nonlinear, independent equations that must be simultaneously solved in order to map the overall efficiency for the transmission.

Results and Discussion

Experimental Coefficients. The goal of this research is to create a typical efficiency map for a hydrostatic transmission. In order to create the map from the previous analysis and modeling, the experimental coefficients shown in Eqs. (17), (19), (31), and (33) must be determined. With the exception of decay constants shown inside the exponential functions (B_1, B_2, and B_3), the remaining coefficients may be determined using a least squares method with a large number of experimental results in which efficiencies, pressures, swash-plate angles, and other relevant parameters have been measured. For instance, the coefficients for the pump flow shown in Eq. (17) may be determined by establishing the following matrix relationships:

$$\underbrace{\begin{bmatrix} \hat{\alpha}_1 \hat{P}_1 & \hat{P}_1 & \sqrt{\hat{P}_1} \\ \hat{\alpha}_2 \hat{P}_2 & \hat{P}_2 & \sqrt{\hat{P}_2} \\ \vdots & \vdots & \vdots \\ \hat{\alpha}_n \hat{P}_n & \hat{P}_n & \sqrt{\hat{P}_n} \end{bmatrix}}_{\mathbf{A}} \underbrace{\begin{Bmatrix} K_0 \\ K_1 \\ K_2 \end{Bmatrix}}_{\mathbf{C}} = \underbrace{\begin{Bmatrix} \hat{\alpha}_1 - \hat{Q}_{p1} \\ \hat{\alpha}_2 - \hat{Q}_{p2} \\ \vdots \\ \hat{\alpha}_n - \hat{Q}_{pn} \end{Bmatrix}}_{\mathbf{F}} \tag{36}$$

where each row in matrix **A** and column vector **F** represents an experiment that has been conducted in the laboratory and where there are a total of n experiments shown. In other words, everything in **A** and **F** is known from experiments. The only unknowns in the Eq. (36) are the coefficient found in the column vector **C**. These, however, may be easily determined using the theory of least squares

$$\mathbf{C} = (\mathbf{A}^{\mathrm{T}} \mathbf{A})^{-1} \mathbf{A}^{\mathrm{T}} \mathbf{F} \tag{37}$$

which produces the best solution for the coefficients given the data in **A** and **F**. This same method can be used to determine most of the experimental coefficients found in Eqs. (19), (31), and (33); however, as previously mentioned, the decay constants inside the exponential functions are not able to be evaluated in this way. Thus, the decay constants were selected by a trial and error method that maximized the R^2 value of the curve fit, which is a measure of the goodness of the curve fit itself.

The coefficients presented in Table 1 have been produced for an existing swash-plate type, axial piston pump, using 840 efficiency measurements and the least squares method previously described. These coefficients produced a R^2 value of 0.925 for the pump volumetric efficiency, and a R^2 value of 0.864 for the pump torque efficiency.

Table 1 Pump coefficients for Eqs. (17) and (19)

Physical meaning	Symbol	Value
Fluid compression	K_0	0.0204
Low Reynolds-number leakage	K_1	0.0151
High Reynolds-number leakage	K_2	0.0109
Static friction	A_p	0.1257
Decay rate for boundary lubrication	B_p	10
Hydrodynamic lubrication	C_p	0.0077
Starting torque	D_p	0.0147

Table 2 Motor coefficients for Eqs. (31) and (33)

Physical meaning	Symbol	Value
Low Reynolds-number leakage	K_3	0.0151
High Reynolds-number leakage	K_4	0.0109
Static friction	A_m	0.1257
Decay rate for boundary lubrication	B_m	10
Hydrodynamic lubrication	C_m	0.0077
Starting torque	D_m	0.0147
Windage losses	E	0.0100

Test data was not available for an axial-piston motor, and therefore the same coefficients that were determined for the pump have been applied to the motor where appropriate. Table 2 lists the coefficients that were used in this study for the motor. An additional coefficient for windage loss has been estimated to be 0.0100. Although the lack of test data for the motor is a weakness of this research, the motor coefficients are not expected to vary considerably from the pump coefficients. Since the primary intention of this work is to illustrate a *method* for mapping the efficiency, this sharing of coefficients between the pump and motor is acceptable. Furthermore, since the pump and motor coefficients will not differ much, the results presented in this paper are deemed to be a good first approximation for an actual transmission.

The following paragraphs will be used to describe the efficiency mapping process for the pump, motor, and transmission as a whole. These mapping efforts are numerical in nature and will use the coefficients that have been presented in Tables 1 and 2.

Pump Efficiency Map. Equations (16), (17), and (19) represent three independent equations that must be solved simultaneously in order to map the efficiency of the pump. These equations are nonlinear and have five unknown parameters within them. These parameters are the pump efficiency, η_p; the fluid pressure, $\hat{P}$; the pump flow, $\hat{Q}_p$; the input-shaft torque, $\hat{T}_p$; and the swash-plate angle of the pump, $\hat{\alpha}$. If two of these five parameters are assumed to be known, then Eqs. (16), (17), and (19) may be simultaneously solved for the other three parameters using a Newton–Raphson numerical method. To generate the efficiency map for the pump, η_p and Q_p were prescribed while solving for the remaining parameters. Figure 4 shows the result of this numerical exercise.

Figure 4 shows the operating regime for the output power of the hydrostatic pump. Like the torque-speed curve of an internal combustion engine, this figure demonstrates a pressure–flow "curve" for the pump. In this figure, the output pressure saturates when we have achieved a maximum pressure setting for the pump, which means that $\hat{P}$ will always remain less than one. On the far right-hand side of Fig. 4, an angled line is shown where the swash-plate angle has saturated as noted by $\hat{\alpha} = 1$. At this line, the pump has reached its maximum capacity for generating flow due to the high Reynolds-number and low Reynolds-number leakages that occur in the pump as a function of pressure, see

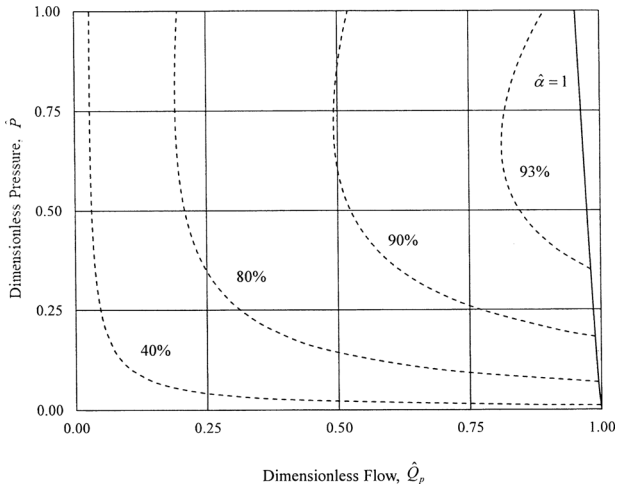

Fig. 4 A typical efficiency map for the hydrostatic pump

Eq. (17). While this angled line looks linear, it is not quite linear due to the presence of the high Reynolds-number flow.

The constant efficiency lines that are shown in Fig. 4 illustrate that at low flow rates the efficiency is independent of fluid pressure, while at low pressures the efficiency is independent of flow. These characteristics are demonstrated by the near vertical and horizontal efficiency lines in these regimes. It is also interesting to note that the maximum efficiency for the pump is not necessarily achieved at the maximum operating pressure. From the results of Fig. 4, it would appear that the pump is most efficient at a mid-pressure range and a high volumetric flow rate. The maximum efficiency for the pump is above 93%.

Motor Efficiency Map. Equations (30), (31), and (33) represent three independent equations that must be solved simultaneously in order to map the efficiency of the motor. Like the pump equations, these equations are nonlinear and have five unknown parameters within them. These parameters are the motor efficiency η_m, the fluid pressure $\hat{P}$, the motor shaft speed $\hat{\omega}_m$, the output shaft torque $\hat{T}_m$, and the swash-plate angle of the pump $\hat{\alpha}$. Again, if two of these five parameters are assumed to be known, then Eqs. (30), (31), and (33) may be simultaneously solved for the other three parameters using a Newton–Raphson numerical method. To generate the efficiency map for the motor, η_m and $\hat{\omega}_m$ were prescribed while solving for the remaining parameters. Figure 5 shows the result of this numerical exercise.

Figure 5 shows the operating regime for the output power of the hydrostatic motor. Again, similar to the torque–speed curve of an internal combustion engine, this figure demonstrates the torque–speed "curve" for the motor. In this figure, the output torque saturates when we have achieved a maximum pressure setting for the transmission, and when other frictional losses subtract from the output of the machine. Equation (33) shows these losses as a nonlinear combination of boundary lubrication, hydrodynamic lubrication, starting torque requirements, and windage losses from within the machine. This saturation line looks flat with respect to shaft speed for most of the operating range, but it is not quite flat due to the nonlinear relationship of these losses. In particular, for slow-speed operation we see a dip in the maximum torque line due to the increased effect of boundary lubrication which becomes significant during high torque (high-pressure/high load), low-speed motor operation. Note: for higher speed operation, friction losses create about a 5% decrease in the maximum torque output of the motor. Once again, on the far right-hand side of Fig. 5 an angled line is shown where the pump swash-plate angle has saturated as noted by $\hat{\alpha} = 1$. The pump swash-plate angle comes into play for this figure due to the fact that the pump supplies the flow to the motor, which in turn turns the motor shaft

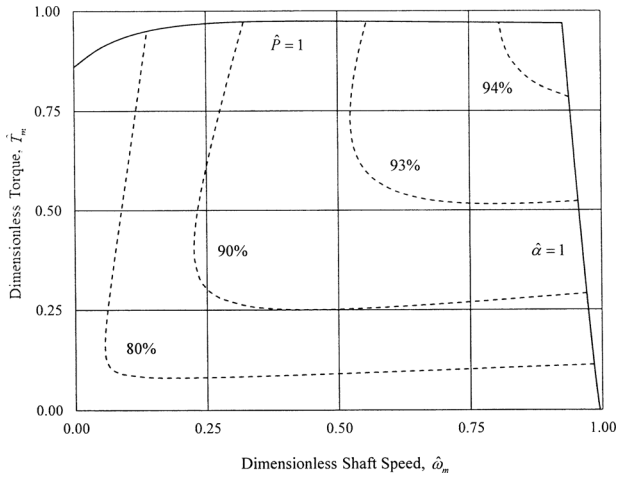

Fig. 5 A typical efficiency map for the hydrostatic motor

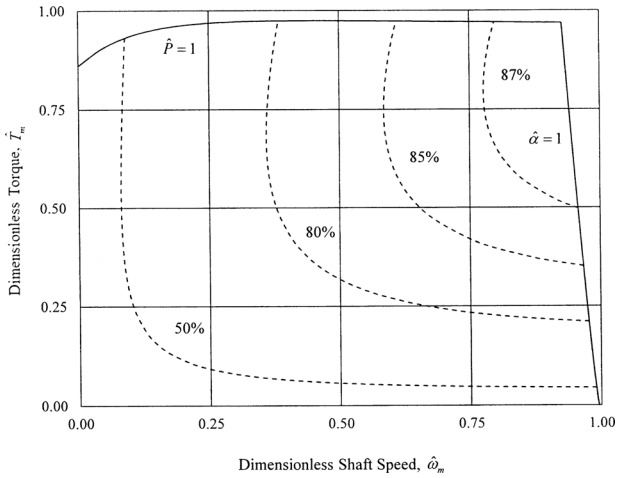

Fig. 6 A typical efficiency map for the hydrostatic transmission

at a given speed, see Eq. (31) for this dependence. When the pump has reached its maximum capacity for generating flow for the motor, the motor output speed becomes limited and this occurs at high pressures when the fluid leakage at the pump and motor is maximum. Again, the angled line in Fig. 5 looks linear, but it is not quite linear due to the presence of the high Reynolds-number flow.

The constant efficiency lines that are shown in Fig. 5 illustrate that at low shaft speeds the efficiency is nearly independent of the output torque, while at low output torque the efficiency is nearly independent of the shaft speed. Again, these characteristics are demonstrated by the near vertical and horizontal efficiency lines in these regimes. From Fig. 5, it may also be observed that the maximum efficiency for the motor is typically experienced at high output torque and high output speed. The maximum efficiency for the motor is above 94%.

Transmission Efficiency Map. Equations (19), (31), (33), and (35) represent four independent equations that must be solved simultaneously in order to map the efficiency of the overall transmission. These equations are nonlinear and have six unknown parameters within them. These parameters are the transmission efficiency, η; the fluid pressure, $\hat{P}$; the motor shaft speed, $\hat{\omega}_m$; the output shaft torque, $\hat{T}_m$; the input-shaft torque, $\hat{T}_p$; and the swash-plate angle of the pump $\hat{\alpha}$. Again, if two of these six parameters are assumed to be known, then Eqs. (19), (31), (33), and (35) may be simultaneously solved for the other four parameters using a Newton–Raphson method. To generate the efficiency map for the transmission, η and $\hat{\omega}_m$ were prescribed while solving for the remaining parameters. Figure 6 shows the result of this numerical exercise.

Figure 6 shows the operating regime for the output power of the hydrostatic transmission. Again, this figure demonstrates the torque–speed "curve" for the transmission, which was the ultimate goal for this research. Because the output torque is limited by the motor, the transmission demonstrates identical saturation characteristics that have already been discussed for the motor. These saturation characteristics are driven by the maximum operating pressure and swash-plate angle of the pump.

As with the pump and motor efficiency characteristics, Fig. 6 illustrates that at low output shaft speeds the efficiency of the transmission is independent of the output torque, while at low output torque the efficiency of the transmission is independent of the output shaft speed. A bit of a visual overlay of Figs. 4 and 5 may be used to see that the overall transmission efficiency characteristics are a compromise between the efficiency characteristics of the pump and the motor. In particular, we see that maximum efficiencies are observed at the high torque and speed points of the map, but that there is a "bringing down" of these points on the torque line due to the operating characteristics of the pump. In other words, it may be said that the maximum efficiency is observed at a mid-to-high output torque of the transmission. The maximum efficiency for the transmission is above 87% with a good share of the operating points remaining above 50%.

Conclusion

The following conclusions are supported by the "Results and Discussion" section of this paper:

(1) That the maximum efficiency of the hydrostatic transmission is above 87%, and is observed near a mid-to-high output torque of the motor and high shaft speeds.
(2) That the transmission usually operates at an operating efficiency of more than 80%.
(3) That at low output shaft speeds the efficiency of the transmission is independent of the output torque.
(4) That at low output torque the efficiency of the transmission is independent of the output shaft speed.

While this paper does not claim to represent the performance characteristics of all hydrostatic transmissions, as these will vary among manufacturers and machine designs, the paper does illustrate a method for creating efficiency maps for these machines that may be used to evaluate the overall efficiency of a system in which they are applied. This evaluation is important for applications where CVT characteristics are being used to increase the efficiency of other components within the system (e.g., the internal combustion engine of an automobile). If the efficiency of the hydrostatic transmission is too low, it may not benefit the overall system to use a device of this sort. On the other hand, if the efficiency gains throughout the system are large, due to the CVT abilities of the hydrostatic transmission, then the use of such a transmission may be viable. This is the decision that a systems engineer must make when considering the use of a hydrostatic transmission for CVT applications. The efficiency maps presented in this research should be helpful toward that end.

Nomenclature

$A_{p,m}$ = the experimental coefficient for modeling static friction for the pump or motor
$B_{p,m}$ = the exponential decay rate for modeling mixed lubrication for the pump or motor
$C_{p,m}$ = the experimental coefficient for modeling hydrodynamic lubrication for the pump or motor
$D_{p,m}$ = experimental coefficient for modeling the starting torque for the pump or motor

$\dot{m}_d$ = mass flow rate on the discharge side of the pump
$\dot{m}_i$ = mass flow rate on the inlet side of the pump
$\dot{m}_{ld}$ = mass flow rate due to leakage on the discharge side of the pump
$\dot{m}_{li}$ = mass flow rate due to leakage on the inlet side of the pump
P = fluid pressure on the high-pressure side of the transmission
P_i = fluid pressure on the inlet side of the pump
Q_m = volumetric flow rate across the motor
Q_p = volumetric flow rate on the discharge side of the pump
Q_i = volumetric flow rate on the inlet side of the pump
Q_{ld} = volumetric flow rate due to leakage on the discharge side of the pump
Q_{li} = volumetric flow rate due to leakage on the inlet side of the pump
$T_{p,m}$ = torque on the input shaft of the pump or motor
U = linear sliding-velocity
V_m = fixed volumetric-displacement of the motor
V_p = maximum volumetric-displacement of the pump
W = load per unit width
$\hat{\alpha}$ = normalized swash-plate angle of the pump
β = fluid bulk modulus-of-elasticity
η = overall efficiency of the transmission
$\eta_{p,m}$ = overall efficiency of the pump or motor
K_n = the nth experimental coefficient for modeling leakage within the transmission
μ = absolute fluid–viscosity
$\mu_{sp,sm}$ = the coefficient-of-friction for the pump or motor as modeled by the Stribeck curve
ρ_d = fluid density on the discharge side of the pump
ρ_i = fluid density on the inlet side of the pump
ρ_o = fluid density at zero gauge-pressure
$\omega_{p,m}$ = angular velocity of the pump or motor shaft

References

[1] Singh, T., 1992, "An Investigation into Power Train Enhancements to Improve Automotive Fuel Economy," M.S. thesis, Wayne State University, Detroit, MI.
[2] EPA Hydraulic Hybrid Research, viewed Jan. 7, 2013, http://www.epa.gov/otaq/technology/research/research-hhvs.htm
[3] Pfiffner, R., Guzzdlla, L., and Onder, C. H., 2003, "Fuel-Optimal Control of CVT Powertrains," Control Eng. Pract., **11**(3), pp. 329–336.
[4] Mapelli, F. L., Tarsitano, D., and Mauri, M., 2010, "Plug-In Hybrid Electric Vehicle: Modeling, Prototype, Realization, and Inverter Losses Reduction Analysis," IEEE Trans. Ind. Electron., **57**(2), pp. 598–607.
[5] Kessels, J. T. B. A., Foster, D. L., and van den Bosch, P. P. J., 2009, "Integrated Powertrain Control for Hybrid Electric Vehicles With Electric Variable Transmission," IEEE Vehicle Power and Propulsion Conference, Dearborn, MI, Sept. 7–10, pp. 376–381.
[6] Ehsani, M., Gao, Y., Gay, S. E., and Emadi, A., 2005, *Modern Electric, Hybrid Electric, and Fuel Cell Vehicles*, CRC, Boca Raton, FL.
[7] Kumar, R., and Ivantysynova, M., 2011, "An Instantaneous Optimization Based Power Management Strategy to Reduce Fuel Consumption in Hydraulic Hybrids," Int. J. Fluid Power, **12**(2), pp. 15–25.
[8] Dirck, M. E., 2003, "The Evaluation and Analysis of a Power Split Hydraulic Hybrid Drivetrain," M.S. thesis, University of Missouri, Columbia, MO.
[9] Vermillion, S. D., 2011, "Modeling a Hydraulic Hybrid Drivetrain: Efficiency Considerations," M.S. thesis, University of Missouri, Columbia, MO.
[10] Al-Ghrairi, T. S., 2012, "Designing and Modeling a Split Torque Hydrostatic Transmission in Series With a Manual Transmission for an Automotive Application," M.S. thesis, University of Missouri, Columbia, MO.
[11] Manring, N. D., 2005, *Hydraulic Control Systems*, Wiley, New York.
[12] Manring, N. D., 2013, *Fluid Power Pumps and Motors: Analysis, Design, and Control*, McGraw-Hill, New York.
[13] Ivantysyn, J., and Ivantysynova, M., 2003, *Hydrostatic Pumps and Motors: Principles, Design, Performance, Modelling, Analysis, Control and Testing*, Tech Books International, New Delhi, India.
[14] Manring, N. D., 1999, "Friction Forces Within the Cylinder Bores of Swash-Plate Type Axial-Piston Pumps and Motors," ASME J. Dyn. Syst. Meas. Control, **121**(3), pp. 531–537.